[17] R. M. Sega and J. D. Norgard, "An infrared measurement technique for the assessment of electromagnetic coupling," *IEEE Trans. Nucl. Sci.*, vol. 32, pp. 4330–4332, NS-1985.
[18] J. D. Norgard, D. C. Fromme, and R. M. Sega, "Correlation of infrared measurement results of coupled fields in long cylinders with a dual series solution," *IEEE Trans. Nucl. Sci.*, vol. 37, no. 6, pp. 2138–2143, Dec. 1990.
[19] T. S. Ibrahim, B. A. Baertlein, R. Gilbert, R. Lee, A. M. Abduljalil, and P.-M. L. Robitaille, "Minimally invasive probing of B1 field distributions in MR coils using infrared sensors," in *Proc. 9th Annu. Meeting Int. Soc. Magnetic Resonance in Medicine*, Glasgow, U.K., 2001, p. 695.
[20] T. S. Ibrahim, R. Gilbert, A. M. Abduljalil, B. A. Baertlein, R. Lee, and P.-M. L. Robitaille, "Measuring RF field distributions in MR coils with IR sensors," in *Proc. IEEE Int. Symp. Antennas and Propagation and USNC/CNC/URSI North American Radio Science*, Boston, MA, 2001, pp. 374–377.
[21] H. Xiao, Y. Zhang, and A. Wang, "Multispectral three-dimensional digital infrared thermal imaging," *Opt. Eng.*, vol. 42, pp. 906–911, 2003.
[22] J. T. Vaughan, H. P. Hetherington, J. O. Otu, J. W. Pan, and J. M. Pohost, "High frequency volume coils for clinical NMR imaging and spectroscopy," *Magn. Reson. Med.*, vol. 32, pp. 206–218, 1994.
[23] P. K. Roschmann, "High-Frequency Coil System for Magnetic Resonance Imaging Apparatus," 4 746 866, 1988, U.S. Patent, assignee.
[24] F. T. Ulaby and P. K. Fung, *Microwave Remote Sensing, Active and Passive: From Theory to Applications*. Dedham, MA: Artech House, 1986.
[25] T. S. Ibrahim, R. Lee, A. M. Abduljalil, B. A. Baertlein, and P.-M. L. Robitaille, "Calculations of EM interactions with biological tissue: magnetic resonance imaging at ultra high field," *Appl. Comput. Electromagn.*, vol. 16, pp. 138–144, 2001.
[26] T. S. Ibrahim, A. Kangarlu, and D. W. Chakeres, "Design and performance issues of RF coils utilized in ultra high field MRI: experimental and numerical evaluations," *IEEE Trans. Biomed. Eng.*, vol. 52, no. 7, pp. 1278–1284, Jul. 2005.
[27] J. P. Berenger, "A perfectly matched layer for the absorption of electromagnetic waves," *J. Comput. Phys.*, vol. 114, pp. 185–20, 1994.
[28] T. S. Ibrahim, C. Mitchell, R. Lee, P. Schmalbrock, and D. W. Chakeres, "a perspective into the operation of RF coils from 1.5 to 11.7 Tesla," *Magn. Reson. Med.*, vol. 54, no. 3, pp. 683–690, 2005.
[29] T. S. Ibrahim, R. Lee, B. A. Baertlein, Y. Yu, and P.-M. L. Robitaille, "On the physical feasibility of achieving linear polarization at high-field: a study of the birdcage coil," in *Proc. 7th Annu. Meeting Int. Soc. Magnetic Resonance in Medicine*, Philadelphia, PA, 1999, p. 2058.
[30] T. S. Ibrahim, R. Lee, B. A. Baertlein, and P.-M. L. Robitaille, "B1 field homogeneity and SAR calculations in the high pass birdcage coil," *Phys. Med. Biol.*, vol. 46, pp. 609–619, 2001.

Novel Parameter Estimation Methods for ^{11}C-Acetate Dual-Input Liver Model With Dynamic PET

Sirong Chen* and Dagan Feng

***Abstract*—The successful investigation of ^{11}C-acetate in positron emission tomography (PET) imaging for marking hepatocellular carcinoma (HCC) has been validated by both clinical and quantitative modeling studies. In the previous quantitative studies, all the individual model parameters were estimated by the weighted nonlinear least squares (NLS) algorithm. However, five parameters need to be estimated simultaneously, therefore, the computational time-complexity is high and some estimates are not quite reliable, which limits its application in clinical environment. In addition, liver system modeling with dual-input function is very different from the widespread single-input system modeling. Therefore, most of the currently developed estimation techniques are not applicable. In this paper, two parameter estimation techniques: graphed NLS (GNLS) and graphed dual-input generalized linear least squares (GDGLLS) algorithms were presented for ^{11}C-acetate dual-input liver model. Clinical and simulated data were utilized to test the proposed algorithms by a systematic statistical analysis. Compared to NLS fitting, these two novel methods achieve better estimation reliability and are computationally efficient, and they are extremely powerful for the estimation of the two potential HCC indicators: local hepatic metabolic rate-constant of acetate and relative portal venous contribution to the hepatic blood flow.**

***Index Terms*—Parameter estimation, ^{11}C-acetate dual-input liver model.**

I. Introduction

The main focus of positron emission tomography (PET) for the study of liver diseases remains on the detection of liver tumors [1]–[3]. Recent clinical studies revealed that the detection of hepatocellular carcinoma (HCC) could be greatly aided by the introduction of ^{11}C-acetate [3]. The successive quantitative modeling studies have conclusively shown that the measurement of the *local hepatic metabolic rate-constant of acetate* (LHMRAct) [4] and the *relative portal venous contribution to the hepatic blood flow* (a_v) [5] from the dynamic PET images can provide important diagnostic information for detecting HCC. In the previous quantitative studies, all the individual model parameters were estimated by the weighted nonlinear least squares (NLS) algorithm. However, five parameters need to be estimated simultaneously [5], which is a difficult task for the weighted NLS. The computational burden is considerable and some estimates are not quite reliable, which limits its application in clinical environment. Therefore, statistically reliable and computationally efficient algorithms are much desired for the ^{11}C-acetate liver model with dual hepatic blood supply.

Several alternative rapid estimation schemes for the use of dynamic PET images have been proposed [6]–[9]. The well-known Patlak method [6] could estimate the LHMRAct. However, the individual

Manuscript received December 31, 2004; revised October 9, 2005. This work was supported by the studentship of the Hong Kong Polytechnic University, and in part by UGC and ARC grants. *Asterisk indicates corresponding author.*

*S. Chen is with the Center for Multimedia Signal Processing, Department of Electronic and Information Engineering, the Hong Kong Polytechnic University, Hong Kong (e-mail: ensrchen@eie.polyu.edu.hk).

D. Feng is with the Center for Multimedia Signal Processing, Department of Electronic and Information Engineering, the Hong Kong Polytechnic University, Hong Kong and also with the School of Information Technologies, the University of Sydney, Sydney, NSW 2006 Australia (e-mail: enfeng@polyu.edu.hk).

Digital Object Identifier 10.1109/TBME.2006.872817

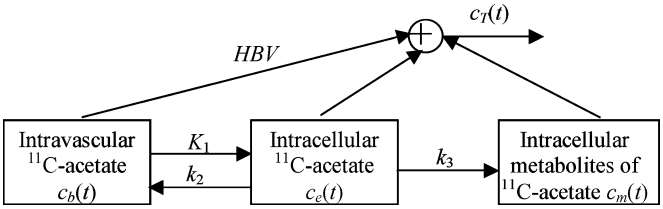

Fig. 1. Three-compartment ^{11}C-acetate liver kinetic model with Parameter a_v in the dual-input function.

parameters are not obtainable, especially a_v which has superior diagnostic value for evaluating HCC. In addition, more accurate estimation of LHMRAct requires the individual a_v value rather than the predetermined fixed a_v value [5]. The integrated projection [7] and the linear least squares (LLS) methods could provide the estimates efficiently, however, they are very biased when applied to the clinical PET images which are noisy and nonuniformly sampled. Although the weighted integration method [8] is generally applicable in clinical settings, it is infeasible to predetermine the optimal weighting functions [9]. Feng *et al.* [9] proposed an unbiased fast parameter estimation algorithm: generalized linear least squares (GLLS) for nonuniformly sampled biomedical system. However, all these techniques are limited in their clinical application to identify the single-input systems, which are not applicable for the dual blood supply liver system. In this paper, two parameter estimation techniques: graphed NLS (GNLS) and graphed dual-input GLLS (GDGLLS) were proposed. The performance of these two algorithms was tested by the clinical and simulated data with comparison to the standard NLS method for the measurement of LHMRAct, a_v and all the other individual model parameters.

II. Methods

The tracer kinetic model describing distribution of labeled ^{11}C-acetate in liver was shown in Fig. 1. In terms of macroparameters, the observed total tissue time activity $c_T(t)$ could be expressed as

$$c_T(t) = (B_1 + B_2 e^{-L_1 t}) \otimes c_b(t) + \mathrm{HBV} \times c_b(t) \tag{1}$$

where

$$B_1 = \frac{K_1 k_3}{k_2 + k_3}, \quad B_2 = \frac{K_1 k_2}{k_2 + k_3}, \quad L_1 = k_2 + k_3$$

are the macroparameters, K_1 (ml/min/ml), k_2 (/min), k_3 (/min) are the rate constants, HBV (ml/ml) is the hepatic blood volume, and $\otimes$ denotes the operation of temporal convolution [5]. The dual-input function $c_b(t)$ was measured by

$$c_b(t) = (1 - a_v) \times c_a(t) + a_v \times c_v(t) \tag{2}$$

where $c_a(t)$ and $c_v(t)$ is the tracer concentration in the hepatic artery (HA) and portal vein (PV), respectively, and a_v is the "relative portal venous contribution to the hepatic blood flow" to be estimated. The LHMRAct was calculated by

$$\mathrm{LHMRAct} = \frac{K_1 k_3}{k_2 + k_3} \tag{3}$$

which has the same form as the forward clearance K.

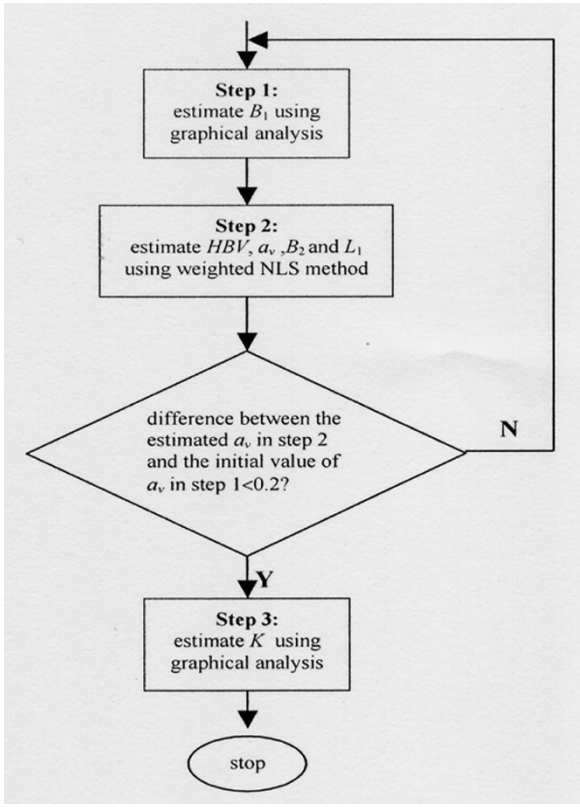

Fig. 2. The flow chart of the GNLS estimation procedure.

A. Graphed Nonlinear Least Squares Algorithm

The proposed GNLS approach applied to the ^{11}C-acetate dual-input liver model has three steps as depicted in Fig. 2. ^{11}C-acetate is metabolized irreversibly with a rate constant of k_3 during the scanning period [4], therefore, beyond the dynamic phase of the dual-input, the ratio of $c_T(t)$ to $c_b(t)$ could be described by

$$\frac{c_T(t)}{c_b(t)} = \frac{K}{c_b(t)} \int_0^t c_b(\tau) d\tau + \frac{K_1 k_2}{(k_2 + k_3)^2} + \mathrm{HBV} \tag{4}$$

where

$$K = \frac{K_1 k_3}{k_2 + k_3}$$

As shown in (1), B_1 has the same form as K, therefore, B_1 could be estimated by a graph of the ratio of $c_T(t)$ to $c_b(t)$ versus the ratio of the blood tracer concentration time integral to $c_b(t)$ during the input steady-state space (3–10 min). In the first step, B_1 was estimated by this linear graphical analysis. To calculate the dual-input function, a_v was empirically set to be 0.8 for the first iteration. During the graphical fitting period (3–10 min), the two blood time-activity curves (TACs) are almost virtually identical [10], therefore, the estimated B_1 is less affected by the individual PV contribution ratio (a_v), and furthermore, it is well accepted that the linear graphical estimates are very robust [6]. Therefore, it is reasonable to consider the estimated B_1 by step 1 as a *prior* for the subsequent estimation schemes. In the second step, the weighted NLS algorithm was utilized to estimate HBV, a_v and the other two macroparameters: B_2 and L_1 with the known B_1, which aims

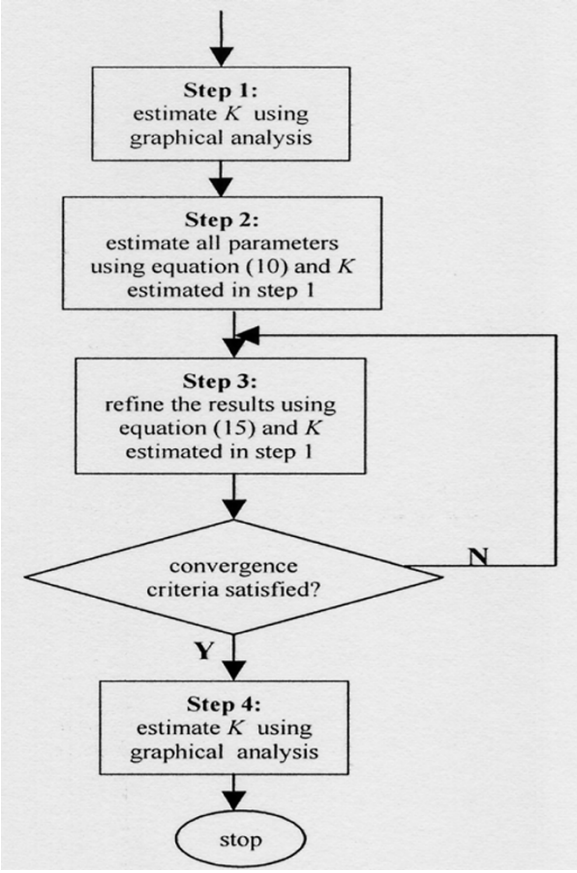

Fig. 3. The flow chart of the GDGLLS algorithm.

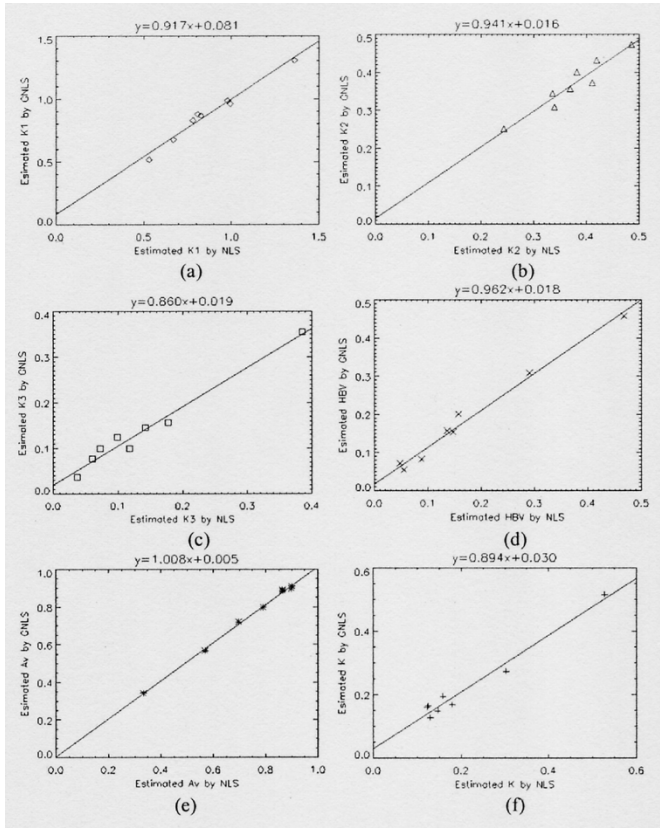

Fig. 4. Correlation of the estimated (a) $\boldsymbol{K}_1$, (b) $\boldsymbol{k}_2$, (c) $\boldsymbol{k}_3$, (d) $\mathbf{HBV}$, (e) $\boldsymbol{a}_v$ and (f) $\boldsymbol{K}$ for the eight clinical ROIs by using GNLS and NLS methods.

to minimize the weighted residual sum of squares. The weight used in this step is

$$w_i = \frac{\Delta t_i}{c_T(t_i)} \quad i = 1, 2, \ldots, 25 \tag{5}$$

where $\Delta t_i = t_i' - t_{i-1}'$ is the scanning interval and $c_T(t_i)$ is the total tracer concentration in tissue at the midtimes of sampling time t_i'. As seen in Fig. 2, the first two steps would not cease until the difference between the estimated a_v in step 2 and the initial value of a_v utilized in step 1 is less than 0.2. In the successive first step estimation, the initial value of a_v would be set to the latest estimated a_v. For nontumor cases, the iteration generally would not be repeated; for tumor cases, one more iteration is generally needed. In the third step, K would be estimated by graphical analysis using the most updated a_v and the fitting period was 3–10 min. By GNLS method, estimates of HBV, a_v and K (LHMRAct) were obtained directly and the model rate constant parameters $K_1 - k_3$ were calculated by

$$\begin{aligned} K_1 &= K + B_2 \\ k_2 &= \frac{B_2 L_1}{K + B_2} \\ k_3 &= \frac{K L_1}{K + B_2} \end{aligned} \tag{6}$$

B. Graphed Dual-Input Generalized Linear Least Squares Algorithm

The first step of the GDGLLS algorithm is the same as the first step GNLS estimation. The model expressed by the second-order differential equation is

$$\begin{aligned} \frac{d^2 c_T(t)}{dt^2} = \mathrm{HBV} \times \frac{d^2 c_b(t)}{dt^2} + [K_1 + (k_2 + k_3)\mathrm{HBV}] \\ \times \frac{dc_b(t)}{dt} + K_1 k_3 \times c_b(t) - (k_2 + k_3) \times \frac{dc_T(t)}{dt} \end{aligned} \tag{7}$$

Substitute $c_b(t)$ in the first term of (7) with (2) and assume the initial conditions were all zeros, we obtain

$$\begin{aligned} c_T(t) = P_0 \times c_a(t) + P_3 (c_v(t) - c_a(t)) + P_1 \int_0^t c_b(\tau) d\tau \\ + K P_2 \int_0^t \int_0^t c_b(\tau) d\tau^2 - P_2 \int_0^t c_T(\tau) d\tau \end{aligned} \tag{8}$$

where

$$\begin{aligned} P_0 &= \mathrm{HBV} \\ P_1 &= K_1 + (k_2 + k_3)\mathrm{HBV} \\ P_2 &= k_2 + k_3 \\ P_3 &= \mathrm{HBV} \times a_v \\ K &= \frac{K_1 k_3}{k_2 + k_3} \end{aligned}$$

Discretize (8) at the midtimes of sampling, the linear equation in matrix form is

$$y = X\theta + \xi \tag{9}$$

where $y = [c_T(t_1), c_T(t_2), \ldots, c_T(t_{25})]^T$, $\theta = [P_0, P_1, P_2, P_3]^T$ are the parameters to be estimated, $\xi = [\xi_1, \xi_2, \ldots, \xi_{25}]^T$ are the equation noise, and X is the coefficient matrix. Assume $\hat{K} \to K, \hat{a}_v \to a_v$, then the equation at bottom of page holds, where $\hat{K}$ was provided by step 1 and $\hat{c}_b(\tau)$ was calculated by (2) with $\hat{a}_v$ (the initial guess of a_v). In the second step, the parameters were estimated by

$$\hat{\theta}_{\mathrm{GDLLS}} = (X^T X)^{-1} X^T y \tag{10}$$

where $\hat{\theta}_{\mathrm{GDLLS}}$ represents the estimated θ in this GDLLS sense. With the estimated K by step 1 and the estimates of $P_0 - P_3$ by (10), $K_1 - k_3$, HBV and a_v could be obtained.

The estimation results of step 2 would be used as the initial values of step 3 aiming to refine the fitting results. If all $c_b(t)$ terms were substituted by (2), the ^{11}C-acetate dual-input model could be described by

$$\begin{aligned}\frac{d^2c_T(t)}{dt^2} &= P_0 \times \frac{d^2c_a(t)}{dt^2} + P_0 a_v \left(\frac{d^2c_v(t)}{dt^2} - \frac{d^2c_a(t)}{dt^2}\right) \\ &\quad + P_1 \times \frac{dc_a(t)}{dt} + P_1 a_v \left(\frac{dc_v(t)}{dt} - \frac{dc_a(t)}{dt}\right) \\ &\quad + KP_2 \times c_a(t) + KP_2 a_v \left(c_v(t) - c_a(t)\right) \\ &\quad - P_2 \times \frac{dc_T(t)}{dt}\end{aligned} \tag{11}$$

where

$$\begin{aligned}P_0 &= \mathrm{HBV} \\ P_1 &= K_1 + (k_2 + k_3)\mathrm{HBV} \\ P_2 &= k_2 + k_3 \\ K &= \frac{K_1 k_3}{k_2 + k_3}\end{aligned}$$

To obtain the GDGLLS solution, assume $\hat{K} \to K$ and $\hat{P}_0 \to P_0, \hat{P}_1 \to P_1, \hat{P}_2 \to P_2$ in the second, fourth, and sixth terms of (11), respectively, we have

$$\begin{aligned}\frac{d^2c_T(t)}{dt^2} &= P_0 \times \frac{d^2c_a(t)}{dt^2} + P_1 \times \frac{dc_a(t)}{dt} + \hat{K}P_2 \times c_a(t) \\ &\quad + a_v \left(\hat{P}_0 \left(\frac{d^2c_v(t)}{dt^2} - \frac{d^2c_a(t)}{dt^2}\right)\right. \\ &\quad \left. + \hat{P}_1 \left(\frac{dc_v(t)}{dt} - \frac{dc_a(t)}{dt}\right)\right. \\ &\quad \left. + \hat{K}\hat{P}_2 \left(c_v(t) - c_a(t)\right)\right) \\ &\quad - P_2 \times \frac{dc_T(t)}{dt}\end{aligned} \tag{12}$$

where $\hat{K}$ is the estimate by step 1 and $\hat{P}_0$, $\hat{P}_1$, and $\hat{P}_2$ represent the most updated estimates of P_0, P_1, and P_2, respectively. Take the Laplace transform of the above equation with the assumption that the initial conditions were all zeros, whiten the correlated equation errors with an autoregressive filter $s(s + \hat{P}_2)$ [9], and then take the inverse Laplace transform, we obtain

$$\begin{aligned}&c_T(t) - \hat{P}_2 \psi_1 \otimes c_T(t) \\ &\quad = P_0 \left(c_a(t) - \hat{P}_2 \psi_1 \otimes c_a(t)\right) + P_1 \psi_1 \otimes c_a(t) \\ &\qquad + P_2 \left(\hat{K}\psi_2 \otimes c_a(t) - \psi_1 \otimes c_T(t)\right) \\ &\qquad + a_v \left(\hat{P}_0 \left(c_v(t) - c_a(t)\right) + (\hat{P}_1 - \hat{P}_0\hat{P}_2)\psi_1\right. \\ &\qquad\quad \left. \otimes (c_v(t) - c_a(t)) + \hat{K}\hat{P}_2 \psi_2 \otimes (c_v(t) - c_a(t))\right)\end{aligned} \tag{13}$$

where

$$\psi_1 = e^{-\hat{P}_2 t}, \quad \psi_2 = \frac{1}{\hat{P}_2}\left(1 - e^{-\hat{P}_2 t}\right)$$

Discretize (13) at the midtimes of sampling, we get

$$r = Z\theta \tag{14}$$

where r is the filtered output, $\theta = [P_0, P_1, P_2, a_v]^T$ are the parameters to be estimated, and Z is the coefficient matrix. In the third step, the parameters would be estimated by

$$\hat{\theta}_{\mathrm{GDGLLS}} = (Z^T Z)^{-1} Z^T r \tag{15}$$

where $\hat{\theta}_{\mathrm{GDGLLS}}$ represents the estimated θ in this GDGLLS sense. The weight used in (15) was by (5) as well. The termination criterion for (15) was that either maximum iteration of 10 was reached or the Euclidean norm of difference of estimates between two successive iterations was less than 0.0001. The flow chart of the GDGLLS algorithm was illustrated in Fig. 3. In the fourth step, Parameter K would be estimated by the graphical analysis with the most updated a_v and the fitting period was 3–10 min.

C. Clinical and Simulation Studies

The clinical image acquisition sequences were as follows: ten frames of 4 s each, eight frames of 10 s each, two frames of 30 s each, followed by three frames of 60 s each and two frames of 120 s each, a total of 25 frames for 10 min. Six patients including two with HCC were studied.

$$X = \begin{bmatrix} c_a(t_1) & \int_0^{t_1} \hat{c}_b(\tau)d\tau & \left(\hat{K}\int_0^{t_1}\int_0^{t_1} \hat{c}_b(\tau)d\tau^2 - \int_0^{t_1} c_T(\tau)d\tau\right) & (c_v(t_1) - c_a(t_1)) \\ c_a(t_2) & \int_0^{t_2} \hat{c}_b(\tau)d\tau & \left(\hat{K}\int_0^{t_2}\int_0^{t_2} \hat{c}_b(\tau)d\tau^2 - \int_0^{t_2} c_T(\tau)d\tau\right) & (c_v(t_2) - c_a(t_2)) \\ \vdots & & & \\ c_a(t_{25}) & \int_0^{t_{25}} \hat{c}_b(\tau)d\tau & \left(\hat{K}\int_0^{t_{25}}\int_0^{t_{25}} \hat{c}_b(\tau)d\tau^2 - \int_0^{t_{25}} c_T(\tau)d\tau\right) & (c_v(t_{25}) - c_a(t_{25})) \end{bmatrix}$$

TABLE I
PARAMETER ESTIMATES OF $\boldsymbol{K}_1$, $\boldsymbol{k}_2$, $\boldsymbol{k}_3$, HBV, $\boldsymbol{a}_v$, AND $\boldsymbol{K}$ BY NLS AND GNLS METHODS FOR THE CLINICAL DATASETS

Datasets	NLS						GNLS					
Number	K_1	k_2	k_3	HBV	a_v	K	K_1	k_2	k_3	HBV	a_v	K
1	0.7815	0.3822	0.0728	0.0880	0.9004	0.1250	0.8307	0.4006	0.0987	0.0817	0.9085	0.1642
2	0.8073	0.3355	0.0602	0.0548	0.8634	0.1228	0.8790	0.3443	0.0768	0.0539	0.8899	0.1603
3	0.5300	0.3694	0.1421	0.2908	0.6972	0.1472	0.5156	0.3573	0.1446	0.3077	0.7192	0.1485
4	0.6687	0.4849	0.1782	0.4680	0.8994	0.1797	0.6749	0.4739	0.1569	0.4568	0.8978	0.1679
5	0.9794	0.2435	0.0371	0.1358	0.7903	0.1296	0.9896	0.2504	0.0366	0.1567	0.7980	0.1261
6	0.8269	0.4194	0.0990	0.0480	0.8657	0.1580	0.8660	0.4316	0.1249	0.0715	0.8837	0.1944
7	1.3601	0.4113	0.1176	0.1573	0.3330	0.3025	1.3055	0.3730	0.0987	0.2006	0.3433	0.2731
8	0.9935	0.3398	0.3852	0.1473	0.5684	0.5278	0.9635	0.3083	0.3547	0.1528	0.5661	0.5154

Note: Datasets 1 to 6 represent nontumor ROIs and 7 to 8 represent HCC ROIs from patients 4 and 6.

TABLE II
COMPARISON OF THE CVS OF THE ESTIMATED $\boldsymbol{K}_1$, $\boldsymbol{k}_2$, $\boldsymbol{k}_3$, HBV, AND $\boldsymbol{a}_v$ BY NLS AND THE ESTIMATED $\boldsymbol{K}$, $\boldsymbol{B}_2$, $\boldsymbol{L}_1$, HBV, AND $\boldsymbol{a}_v$ BY GNLS FOR THE CLINICAL DATASETS

Datasets	NLS					GNLS				
Number	K_1	k_2	k_3	HBV	a_v	K	B_2	L_1	HBV	a_v
1	18.40	30.45	35.64	52.80	7.70	9.70	24.79	22.16	59.45	7.86
2	8.01	15.65	29.84	53.97	8.46	25.01	8.54	8.69	59.19	7.56
3	9.74	21.46	22.40	18.45	10.45	9.20	10.27	9.18	15.33	8.94
4	15.87	25.88	14.66	16.65	5.31	8.39	13.73	10.02	14.23	4.99
5	9.80	18.86	71.47	60.41	13.39	38.95	10.17	12.38	51.14	11.89
6	22.44	36.03	33.22	172.6	12.74	10.06	23.47	19.99	141.7	11.44
7	15.71	24.53	17.08	52.18	74.25	12.17	15.96	13.88	50.16	73.23
8	43.88	63.92	29.20	77.70	51.17	2.82	31.96	18.79	39.51	21.12
Average	17.98	29.60	31.69	63.10	22.93	14.54	17.36	14.39	53.84	18.38

For each patient, one nontumor region-of-interest (ROI) in liver was extracted. Two HCC ROIs were extracted from the two patients suffered from HCC. To obtain the hepatic dual inputs on the dynamic PET images, the TAC of PV was evaluated by direct activity-time measurement and the TAC of HA was approximated by evaluating the TAC of the abdominal aorta adjacent to the liver. To reduce the radioactivity spillover effect from the adjacent tissue, the last five measurements of the TAC of PV were replaced by the corresponding HA data in this study.

All the parameter estimation methods including NLS, GNLS and GDGLLS were tested by computer simulated data. Two simulated datasets (one representing HCC) with the same image-derived dual inputs extracted from clinical data were generated according to (1). A pseudorandom number generator was used to generate the Gaussian noise added to the calculated TAC and the variance structure is

$$\sigma^2(t_i) = \frac{\alpha \times c_T(t_i)}{\Delta t_i} \quad i = 1, 2, \ldots, 25 \tag{16}$$

where $c_T(t_i)$ is the calculated TAC, Δt_i is the scanning interval (same as clinical study), and α is the proportional constant representing the noise level.

TABLE III
AICS AND SCS BY NLS AND GNLS ALGORITHMS FOR THE CLINICAL DATASETS

Datasets	NLS		GNLS	
Number	AIC	SC	AIC	SC
1	176.51	182.61	178.74	183.61
2	165.97	172.07	166.68	171.56
3	179.84	185.94	178.58	183.45
4	163.61	169.71	163.82	168.70
5	177.61	183.71	177.12	182.00
6	176.32	182.41	176.46	181.34
7	192.54	198.63	194.04	198.92
8	169.44	175.54	167.60	172.47

D. Statistical Criteria

For the clinical datasets, the correlation analysis was conducted for the estimated $K_1 - k_3$, a_v, HBV and K provided by NLS and GNLS

TABLE IV
ESTIMATION RESULTS OF K_1, k_2, k_3, HBV, a_v, AND K FROM TWO SETS OF SIMULATION. THE TRUE VALUE OF THE TWO DATASETS IS $K_1 = 0.65, k_2 = 0.40, k_3 = 0.15$, HBV $= 0.30$, $a_v = 0.75$, AND $K_1 = 1.35, k_2 = 0.35, k_3 = 0.13$, HBV $= 0.30$, $a_v = 0.40$ (REPRESENTING HCC), RESPECTIVELY. THE ESTIMATED PARAMETERS REPRESENT THEIR MEAN VALUES. THE MEAN VALUES, ***biases*** (PERCENTAGE VALUE), AND **CVs** (PERCENTAGE VALUE) WERE CALCULATED FROM 200 SIMULATION RUNS

Method	K_1	$bias_1$	CV_1	k_2	$bias_2$	CV_2	k_3	$bias_3$	CV_3	HBV	$bias_H$	CV_H	a_v	$bias_a$	CV_a	K	$bias_K$	CV_K
	Noise level α=0.1																	
NLS	0.6504	0.06	0.75	0.4007	0.17	1.45	0.1502	0.17	1.19	0.2998	0.07	1.77	0.7498	0.02	0.96	0.1774	0.06	0.48
GNLS	0.6587	1.34	0.45	0.4157	3.93	0.62	0.1559	3.94	0.72	0.2952	1.59	1.59	0.7472	0.37	0.94	0.1796	1.32	0.30
GDG*	0.6505	0.07	0.57	0.4090	2.24	0.90	0.1568	4.55	0.72	0.3040	1.34	1.67	0.7508	0.11	1.04	0.1796	1.31	0.31
	Noise level α=0.5																	
NLS	0.6516	0.24	3.90	0.4030	0.75	7.51	0.1510	0.63	5.99	0.2992	0.28	8.93	0.7479	0.28	4.92	0.1776	0.16	2.39
GNLS	0.6577	1.19	2.32	0.4153	3.82	3.21	0.1562	4.14	3.58	0.2953	1.56	8.55	0.7453	0.62	4.30	0.1797	1.37	1.53
GDG	0.6504	0.05	2.98	0.4083	2.07	4.61	0.1562	4.16	3.59	0.3018	0.61	8.90	0.7441	0.79	4.58	0.1791	1.05	1.56
	Noise level α=1																	
NLS	0.6526	0.40	8.21	0.4054	1.36	15.80	0.1509	0.58	12.22	0.2973	0.89	18.14	0.7410	1.21	10.62	0.1771	0.13	4.97
GNLS	0.6543	0.66	5.02	0.4125	3.12	7.08	0.1566	4.39	7.26	0.2954	1.53	16.20	0.7386	1.52	10.08	0.1797	1.38	3.06
GDG	0.6448	0.80	6.11	0.4029	0.73	9.57	0.1557	3.82	7.19	0.2978	0.72	18.12	0.7268	3.09	12.00	0.1785	0.70	3.15
	Noise level α=2																	
NLS	0.6527	0.42	17.89	0.4100	2.50	33.56	0.1492	0.54	25.41	0.2932	2.27	36.45	0.7088	5.50	28.83	0.1740	1.87	11.31
GNLS	0.6421	1.22	10.25	0.3993	0.18	14.87	0.1562	4.14	14.99	0.2880	4.00	35.28	0.7003	6.63	26.12	0.1794	1.18	6.24
GDG	0.6185	4.85	13.01	0.3822	4.44	22.28	0.1585	5.69	16.34	0.2877	4.09	36.00	0.6826	8.98	30.26	0.1785	0.70	5.81
Method	K_1	$bias_1$	CV_1	k_2	$bias_2$	CV_2	k_3	$bias_3$	CV_3	HBV	$bias_H$	CV_H	a_v	$bias_a$	CV_a	K	$bias_K$	CV_K
	Noise level α=0.1																	
NLS	1.3504	0.03	0.89	0.3503	0.09	1.58	0.1301	0.10	1.29	0.3000	0.01	2.39	0.4000	0.00	3.56	0.3658	0.04	0.55
GNLS	1.3556	0.41	0.73	0.3544	1.25	1.01	0.1320	1.56	0.68	0.2997	0.11	2.04	0.4016	0.40	3.01	0.3680	0.64	0.32
GDG	1.3770	2.00	0.64	0.3733	6.65	0.85	0.1421	9.31	0.74	0.3111	3.71	2.01	0.4144	3.60	3.34	0.3684	0.77	0.32
	Noise level α=0.5																	
NLS	1.3507	0.05	4.54	0.3515	0.42	8.04	0.1305	0.39	6.49	0.3000	0.00	11.70	0.3960	1.01	18.39	0.3657	0.03	2.80
GNLS	1.3531	0.23	3.73	0.3538	1.08	5.14	0.1321	1.60	3.44	0.3000	0.01	10.46	0.3972	0.70	16.05	0.3677	0.57	1.63
GDG	1.3724	1.66	3.24	0.3720	6.29	4.29	0.1423	9.46	3.78	0.3102	3.39	10.61	0.4146	3.65	16.86	0.3681	0.68	1.61
	Noise level α=1																	
NLS	1.3501	0.01	9.31	0.3533	0.95	16.49	0.1308	0.58	13.19	0.3009	0.31	23.01	0.3842	3.96	39.52	0.3645	0.30	5.82
GNLS	1.3471	0.21	7.70	0.3531	0.88	10.82	0.1326	2.00	7.10	0.3011	0.39	20.60	0.3844	3.90	36.20	0.3673	0.46	3.28
GDG	1.3630	0.96	6.45	0.3695	5.57	8.56	0.1429	9.93	7.88	0.3125	4.17	21.51	0.4007	0.17	35.73	0.3674	0.50	3.22
	Noise level α=2																	
NLS	1.3509	0.07	17.82	0.3596	2.76	31.15	0.1313	0.98	26.34	0.3071	2.36	44.60	0.3475	13.12	91.11	0.3588	1.86	12.69
GNLS	1.3283	1.61	15.27	0.3502	0.06	21.41	0.1344	3.38	14.90	0.3087	2.91	40.53	0.3477	13.08	86.68	0.3658	0.05	6.65
GDG	1.3309	1.41	13.02	0.3619	3.39	17.30	0.1467	12.83	19.20	0.3203	6.76	40.63	0.3497	12.57	86.67	0.3658	0.06	6.46

Note: "GDG" are the abbreviations of "GDGLLS".

methods, and additionally the Akaike information criteria (AIC) [11] and Schwarz criteria (SC) [12] were utilized to test the "goodness of fit." The reliability of parameter estimation was accessed by the coefficient of variation (CV) formulated as

$$\mathrm{CV}_P = \frac{\mathrm{SD}_P}{P} \times 100\% \tag{17}$$

where P is the parameter estimate and SD_P is the standard deviation (SD) of P. For clinical study, SDs were estimated as the square roots of the diagonal elements of the covariance matrix and the covariance matrix was estimated based on sensitivity functions. For the simulation study, the accuracy of the estimated parameters was evaluated by *bias*.

III. RESULTS AND DISCUSSION

To evaluate the performance of GNLS, comparison between the estimation by NLS and GNLS for clinical datasets was conducted. The parameter estimates of $K_1 - k_3$, HBV, a_v, and K (LHMRAct) by NLS and GNLS were listed in Table I. In Table I, the estimation results

TABLE V
AVERAGE NUMBER OF ITERATIONS NEEDED BY GDGLLS IN SIMULATION STUDY

Datasets Number	Noise level 0.1	0.5	1	2
1	2.99	2.77	3.23	4.12
2	3.98	3.58	3.48	3.91

predicted by the two methods are comparable with each other. The correlation coefficients by correlation analysis of the two sets of K_1, k_2, k_3, HBV, a_v, and K (LHMRAct) are 0.9872, 0.9563, 0.9868, 0.9920, 0.9987, and 0.9847, respectively, and the correlation was plotted in Fig. 4. As shown in Fig. 4, all the estimated parameters by the two approaches correlated closely with each other. For the six nontumor ROIs, the estimated a_v expressed as $\mathrm{mean} \pm \mathrm{SD}$ are 0.8495 ± 0.0752 and 0.8361 ± 0.0790 by GNLS and NLS methods, respectively; whereas the estimated K by GNLS and NLS methods are 0.1602 ± 0.0225, and

0.1437 ± 0.0224, respectively. The CVs of the estimated K_1, k_2, k_3, HBV, and a_v by NLS and the estimated K, B_2, L_1, HBV, and a_v by GNLS for the clinical datasets were summarized in Table II. The average CVs of K, B_2, and L_1 are much less than the mean CVs of K_1, k_2 and k_3 by NLS (referred to Table II). $K_1 - k_3$ were calculated by (6) with the estimated K, B_2, and L_1, therefore, they could be much more reliably estimated by the proposed GNLS method. It is worth noting in Table II that the majority of the CVs of the estimated a_v by GNLS are less than those by NLS, and the estimated a_v of region 8 is considerably more reliable. The estimation of HBV by GNLS is generally more reliable than that by NLS especially for region 8. As displayed in Table III, compared to NLS method all SCs by GNLS except those of regions 1 and 7 are smaller, indicating that GNLS could provide better fit. The two sets of AICs are comparable with each other. During the GNLS fitting, owing to the reduced number of parameters to be estimated by the recursive NLS procedure, the computational burden is reduced. Since B_1 are predetermined and considered as a *prior*, the fitting results of the second step regression are less affected by the initial guess.

The estimation results of $K_1 - k_3$, HBV, a_v, and K (LHMRAct) calculated from 200 simulation runs by NLS, GNLS, and GDGLLS were presented in Table IV. When compared with NLS method, $K_1 - k_3$ could be considerably more reliably estimated by both GNLS and GDGLLS especially when the noise level is high. Nevertheless, NLS could provide more accurate estimates of $K_1 - k_3$. As shown in Table IV, the estimation of a_v and HBV by the two proposed methods is moderately more reliable than that by NLS. The accuracy of the estimated a_v and HBV by using the two presented approaches is in general comparable with that of NLS. In Table IV, the estimation of K by both GNLS and GDGLLS is much more reliable than that by NLS for all the cases, especially when the noise level is 2. The estimation accuracy of K by the two methods is satisfactory since all $biases$ are around 1% for dataset 1 and less than 1% for dataset 2. When the noise level is 2, both methods could achieve better fitting accuracy than NLS for K. It could be seen in Table IV that the estimation accuracy of all the parameters by the two presented techniques is generally not sensitive to the noise level, which may be extremely useful in clinical settings whose noise level is generally high. When comparing the CVs in Tables II (clinical study) and IV (simulation study), simulated data with noise level 2 seems comparable with the clinical data. All the individual model parameters could be expressed analytically in terms of the PET measurements by GDGLLS algorithm, therefore this fitting procedure is very fast. The average number of iterations needed for step 3 of GDGLLS is generally less than 4 (referred to Table V). As shown in Table V, when the noise level increases, the number of iterations needed would not increase which may be very valuable in clinical noisy environment.

IV. Conclusion

Two novel parameter estimation techniques for $^{11}\mathrm{C}$-acetate dual-input liver model using dynamic PET images were presented in this study. Compared to NLS approach, more reliable parameter estimates and better fitting quality in terms of SC could be provided by GNLS method for clinical study, and the computational burden of GNLS is reduced. GDGLLS algorithm could generally identify all the parameters more reliably than NLS and the fitting procedure is very fast. Compared to NLS fitting, both presented algorithms could achieve a comparable estimation accuracy of the two HCC indicators. When the noise level is 2, both methods could even achieve better fitting accuracy of K. Therefore, in addition to the robustness and computational efficiency, the two estimation algorithms could provide better ways for the early detection of HCC.

Acknowledgment

The authors would like to express their sincere gratitude to B. Parker for his kind help.

References

[1] S. Okazumi, K. Isono, K. Enomoto, T. Kikuchi, M. Ozaki, H. Yamamoto, H. Hayashi, T. Asano, and M. Ryu, "Evaluation of liver tumors using fluorine-18-fluorodeoxyglucose PET: characterization of tumor and assessment of effect of treatment," *J. Nucl. Med.*, vol. 33, no. 3, pp. 333–339, 1992.

[2] T. Torizuka, N. Tamaki, T. Inokuma, Y. Magata, Y. Yonekura, A. Tanaka, Y. Yamaoka, K. Yamamoto, and J. Konishi, "Value of fluorine-18-FDG-PET to monitor hepatocellular carcinoma after interventional therapy," *J. Nucl. Med.*, vol. 35, no. 12, pp. 1965–1969, 1994.

[3] C.-L. Ho, S. Yu, and D. Yeung, "$^{11}\mathrm{C}$-acetate PET imaging in hepatocellular carcinoma and other liver masses," *J. Nucl. Med.*, vol. 44, no. 2, pp. 213–221, 2003.

[4] S. Chen, C. Ho, D. Feng, and Z. Chi, "Tracer kinetic modeling of $^{11}\mathrm{C}$-acetate applied in the liver with positron emission tomography," *IEEE Trans. Med. Imag.*, vol. 23, no. 4, pp. 426–432, Apr. 2004.

[5] S. Chen and D. Feng, "Noninvasive quantification of the differential portal and arterial contribution to the liver blood supply from PET measurements using $^{11}\mathrm{C}$-acetate kinetic model," *IEEE Trans. Biomed. Eng.*, vol. 51, no. 9, pp. 1579–1585, Sep. 2004.

[6] C. S. Patlak, R. G. Blasberg, and J. D. Fenstermacher, "Graphical evaluation of blood-to-brain transfer constants from multiple-time uptake data," *J. Cereb. Blood Flow Metab.*, vol. 3, pp. 1–7, 1983.

[7] S. C. Huang, R. E. Carson, and M. E. Phelps, "Measurement of local blood flow and distribution volume with short-lived isotopes: a general input technique," *J. Cereb. Blood Flow Metab.*, vol. 2, pp. 99–108, 1982.

[8] R. E. Carson, S. C. Huang, and M. V. Green, "Weighted integration method for local cerebral blood flow measurements with positron emission tomography," *J. Cereb. Blood Flow Metab.*, vol. 6, pp. 245–258, 1986.

[9] D. Feng, S. C. Huang, Z. Wang, and D. Ho, "An unbiased parametric imaging algorithm for nonuniformly sampled biomedical system parameter estimation," *IEEE Trans. Med. Imag.*, vol. 15, no. 4, pp. 512–518, Aug. 1996.

[10] O. L. Munk, L. Bass, K. Roelsgaard, D. Bender, S. B. Hansen, and S. Keiding, "Liver kinetics of glucose analogs measured in pigs by PET: importance of dual-input blood sampling," *J. Nucl. Med.*, vol. 42, no. 5, pp. 795–801, 2001.

[11] H. Akaike, "A new look at the statistical model identification," *IEEE Trans. Automat. Contr.*, vol. AC-19, pp. 716–723, 1974.

[12] G. Schwarz, "Estimating the dimension of a model," *Ann. Statist.*, vol. 6, pp. 461–564, 1978.